Structure, Spectroscopy, and Microscopic Model of Tubular Carbocyanine Dye Aggregates

Cătălin Didraga,[†] Audrius Pugžlys,[†] P. Ralph Hania,[†] Hans von Berlepsch,[‡] Koos Duppen,[†] and Jasper Knoester*,[†]

Materials Science Centre, University of Groningen, Nijenborgh 4, 9747 AG Groningen, The Netherlands, and Forschungszentrum für Elektronenmikroskopie, Freie Universität Berlin, Fabeckstrasse 36a, D-14195 Berlin, Germany

Received: April 20, 2004; In Final Form: June 30, 2004

Self-assembled cylindrical aggregates of amphiphilic carbocyanine dye molecules are interesting candidates for synthetic light-harvesting systems and electronic energy transport wires. To be able to optimize the properties of such systems, detailed information on the molecular structure as well as the static and dynamic optical properties is required. We report cryo-transmission electron microscopy (cryo-TEM) experiments on 3,3′-bis(3-sulfopropyl)-5,5′,6,6′-tetrachloro-1,1′-dioctylbenzimidacarbocyanine (C8S3) aggregates that reveal a double-layer tubular structure. By combining these results with information from both isotropic and polarized spectral responses, a detailed molecular picture of these aggregates is obtained. The basis of our theoretical analysis of the spectroscopic data is the formation of the inner and outer cylinders by rolling cyanine sheets with a brick-layer structure onto cylindrical surfaces with diameters of 11 and 16 nm. This model very well reproduces the spectral properties of the excitonic transitions of the C8S3 aggregates. The combination of experimental and theoretical techniques for the first time provides detailed insight into the molecular arrangement inside these aggregates.

I. Introduction

The preparation of low-dimensional supramolecular systems with controlled structure and optical dynamics is a topic of considerable current interest.[1,2] Such systems can serve as artificial light harvestors, in analogy with natural antenna complexes in photosynthetic systems,[3−5] and as transport wires of electronic excitation energy. In addition, they can be used to create devices with tunable and strongly anisotropic optical properties, such as a strong circular dichroism based on a possible chirality in the supramolecular arrangement. In search of such new materials, the family of substituted 5,5′,6,6′-tetrachlorobenzimidacarbocyanine dyes (Figure 1) recently has stirred special interest.[6] This is due to the possibility of tuning the morphology of the aggregates formed from these chromophores by (small) changes in their side chains and their environment. Thus, aggregates with planar, spherical, and cylindrical (tubular) morphologies have been prepared.[7,8] These different shapes give rise to strong variations in the optical properties. These variations do not arise from changes in the electronic structure of the individual chromophores; the side chains and environment hardly affect the π system of a single chromophore.[9] Rather, these variations result from the influence of the side chains and the solvent on the packing of the dye molecules in the aggregates. By influencing the intermolecular interactions and the spatial arrangement of dipole orientations, the packing has a strong effect on the collective optical properties of the molecules within an aggregate.

Thus far, it has been found to be difficult to relate the changes in the optical properties directly to changes in the microscopic molecular arrangement. The reason is that, although changes in aggregate morphology can be readily observed using cryo-transmission electron microscopy (cryo-TEM),[7,8,10] this technique lacks the spatial resolution to provide insight into the aggregate structure at the molecular scale. It is the aim of this paper to present the first detailed exploration of the relationship between morphology, structure, and optical properties for one type of tetrachlorobenzimidacarbocyanine aggregate, namely, for the tubular aggregates formed in the case of 1,1′-dioctyl and 3,3′-bis(3-sulfopropyl) subsituents (abbreviated by C8S3 in Figure 1). The reason for our special interest in these tubular aggregates is that they closely resemble the rod elements in the light-harvesting chlorosomes of green bacteria[11−14] and exhibit a rigid wire structure that might be suitable for energy transport.

To appreciate the variation of morphologies and related optical properties, it is useful to briefly review recent studies on the aggregates of several of the derivatives of the 5,5′,6,6′-

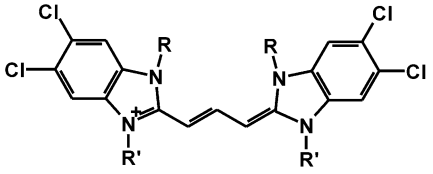

R	R′	Counterion	Abbreviation
C_2H_5	C_2H_5	Cl^-	TTBC
C_2H_5	$(CH_2)_4SO_3^-$	Na^+	TDBC
C_8H_{17}	$(CH_2)_3COOH$	Br^-	C8O3
C_8H_{17}	$(CH_2)_4COOH$	Br^-	C8O4
C_8H_{17}	$(CH_2)_3SO_3^-$	Na^+	C8S3

Figure 1. Chemical structure of the 5,5′,6,6′-tetrachlorobenzimidacarbocyanine dyes with their abbreviated names.

* Corresponding author. Fax: 31-50-3634947. E-mail: knoester@phys.rug.nl.
[†] University of Groningen.
[‡] Freie Universität Berlin.

10.1021/jp048288s CCC: $27.50
Published on Web 08/26/2004

tetrachlorobenzimidacarbocyanine chromophore shown in Figure 1. The frequently studied dye TDBC [1,1′-diethyl, 3,3′-bis(4-sulfobutyl) substituents] forms sheetlike aggregates[7] that reveal an absorption spectrum dominated by one intense sharp J band centered at 587 nm.[15] On the other hand, the dye C8O4 [1,1′-dioctyl and 3,3′-bis(4-carboxybutyl) substituents] forms stacks of bilayered ribbons, with an absorption spectrum that strongly resembles that of TDBC, although the shape of the J band changes.[7] Finally, the dye C8O3, in which just a very small change occurs relative to C8O4, namely, the 3,3′-nitrogen substituents are changed from bis(4-carboxybutyl) to bis(3-carboxypropyl), self-assembles into superhelical aggregates of tubular strands with a total thickness of a few tens of nanometers and lengths of hundreds of nanometers. Each strand represents a double-wall tubule of total diameter 10−11 nm with a double-wall thickness of 4.0 ± 0.5 nm.[7,10] We note in passing that double-wall cylindrical aggregates also occur as natural light-harvesting complexes.[16] The optical properties of the C8O3 aggregates are quite rich: they exhibit four J-type absorption bands.[10] Moreover, it was shown that the addition of short-chain alcohols to a C8O3/water solution leads to the formation of thicker and longer superhelices,[17] whereas addition of poly(vinyl alcohol) (PVA) causes a dismantling of the superhelices into separate strands with a slightly increased thickness.[10] Alternatively, adding the anionic surfactant sodium dodecyl sulfate to a C8O3/water solution initially gives single-wall tubules, which over the course of several days, are twisted into thick multilamellar tubes.[8] All of these modifications in the aggregate morphology lead to changes in the species' optical properties, in particular, in the number, positions, and relative strengths of the absorption bands.

The first observation of the C8O3 absorption spectra with two or three J bands was reported in ref 18 and, using a simple exciton model, could be directly related to a cylindrical morphology. The polarization of the various exciton transitions relative to the aggregate axis, as could be determined in a stretched polymer film, added support to the model and the assignment of the J bands. Because the samples studied in ref 18 contained short-chain alcohols in the solution, the C8O3 aggregates were recently reinvestigated, now revealing four J bands,[10] once again underlining the strong effects of additives on the aggregation process. Aligning the helices in streaming solution showed that three of these bands are polarized parallel to the aggregate alignment and one perpendicular to it. The C8O3 superhelices also exhibit a pronounced CD spectrum.[19−21]

Despite all of this previous work, no detailed structural model has been reported that explains the number, positions, polarization directions, and relative strengths of the absorption bands observed for the tubular tetrachlorobenzimidacarbocyanine aggregates. Generic exciton models have been used to explain the rough features of the linear absorption, linear dichroism, and pump−probe spectra.[18,22−24] Although of interest, these models contained too much freedom to reveal detailed microscopic information, such as the packing of the molecules in the aggregate. This is in sharp contrast to the situation of the tubular aggregates that occur in the chlorosomes of green bacteria, for which the molecular arrangement is known rather well[13,14] and many of the spectroscopic details have been described successfully using exciton theory.[25,26]

In this paper, we aim to reach a similar level of understanding for tubular aggregates formed by one of the 5,5′,6,6′-tetrachlorobenzimidacarbocyanine derivatives. The dye we have studied is C8S3. The reason to study this derivative, instead of C8O3, is that, in pure water, these chromophores turn out to form *isolated* double-wall tubules, which are simpler to model than the complicated superhelical arrangements of tubules formed by C8O3. The absence of interactions between individual tubules obviously reduces the number of unknown parameters in the model. We report cryo-TEM data, as well as isotropic and polarized absorption spectra, for C8S3 aggregates and show that an exciton model based on the wrapping of a brick-layer structure[27−29] for the molecular arrangement on the inner and outer cylinder walls explains the observed spectra. As a result, for the first time, a reliable microscopic picture is given of tubular carbocyanine aggregates.

The outline of this paper is as follows: In section II, we briefly address the materials used and the sample preparation, as well as the methods employed to measure the spectra. In section III, we present the morphology of the C8S3 aggregates as revealed by cryo-TEM and the measured isotropic and polarized absorption spectra. In section IV, we first describe the structure obtained when a brick layer is rolled onto a cylinder wall and then present the exciton Hamiltonian on this structure, give general expressions of the various spectra of interest in terms of the eigenstates of this Hamiltonian, and finally address the incorporation of energetic disorder into the model. Explicit results of the exciton model, in particular tuned toward an understanding of the experimentally obtained spectra for C8S3 aggregates, are presented and discussed in section V. Finally, in section VI, we present our conclusions.

II. Materials and Methods

The synthesis, purification, and analytical characterization of the dye C8S3 and the other 5,5′,6,6′-tetrachlorobenzimidacarbocyanine derivatives is described in detail in ref 6. The dye C8S3 consisting of its betain salt was supplied by FEW Chemicals (Wolfen, Germany) and was used as received. The molecular mass is 902.8 g/mol. The molar extinction coefficient in dimethyl sulfoxide (DMSO) was found to be 1.40×10^5 L/(mol·cm).

To form aggregates, the dye was dissolved in doubly distilled deionized water, forming 0.35 mM stock solutions. The samples for cryo-TEM were prepared at room temperature by placing a droplet (10 μL) of the stock solution on a hydrophilized perforated carbon filmed grid (60-s plasma treatment at 8 W using a BALTEC MED 020 device). The excess fluid was blotted off to create an ultrathin layer (typical thickness of 100 nm) of the solution spanning the holes of the carbon film. The grids were immediately vitrified in liquid ethane at its freezing point (−184 °C) using a standard plunging device. Ultrafast cooling is necessary for an artifact-free thermal fixation (vitrification) of the aqueous solution avoiding crystallization of the solvent or rearrangement of the assemblies. The vitrified samples were transferred under liquid nitrogen into a Philips CM12 transmission electron microscope using the Gatan cryo-holder and -stage (model 626). Microscopy was carried out at the −175 °C sample temperature using the microscope's low-dose protocol at a primary magnification of 58300×. The defocus was chosen in all cases to be 0.9 μm, corresponding to a first zero of the phase contrast transfer function at 1.8 nm.

Spectroscopic experiments were performed at room temperature using white light, generated in a 2-mm sapphire plate by pumping with 120-fs, 800-nm pulses originating from a 1-kHz Ti:sapphire laser system (Hurricane, Spectra Physics). The energy of the incident light and of the light transmitted through the sample was monitored via a polychromator by an OMA system (Princeton Instruments). The linear dichroism (LD) spectra were calculated as the difference between the absorption

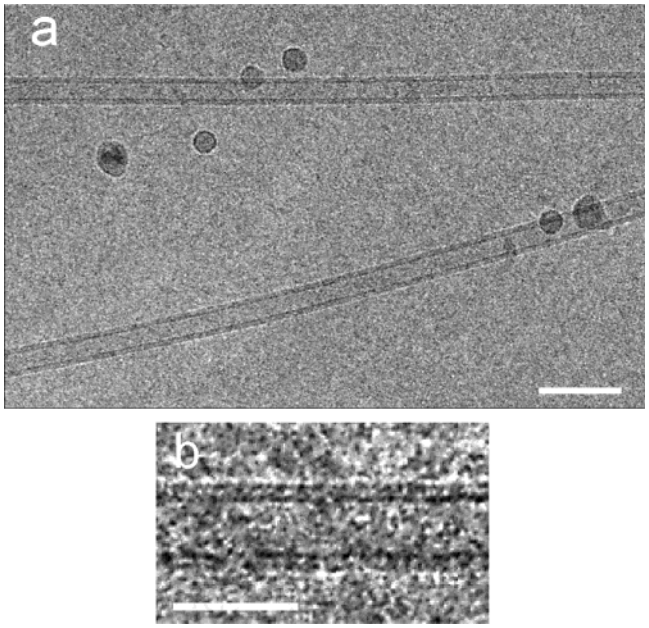

Figure 2. (a) Cryo-TEM image of bilayered tubular C8S3 aggregates. (b) At higher magnification, the constituting chromophore monolayers become visible. Bars: (a) 50 and (b) 20 nm.

spectra measured for light polarized parallel and perpendicular to the direction of an aligning flow. The flow was created by a peristaltic pump (Cole-Parmer's Masterflex), which pumped the aggregated dye solutions through a 100-μm-thick and 1-cm-wide fused silica cell. The measurement of the LD spectrum as a function of the flow rate revealed maximum alignment of the aggregates already at relatively low flow rates. For example, saturation of the alignment of pure C8O3 aggregates[10] is reached at a flow rate of about 0.5 cm^3/s or a flow velocity of 50 cm/s. The measurements presented here were performed for maximum alignment of the sample, i.e., at a flow rate of about 2 cm^3/s.

Fluorescence spectra were recorded using a luminescence spectrometer (Perkin-Elmer LS50B). The fluorescence was detected in a front face geometry, with excitation and emission slits set at 3 nm. In these experiments, the sample solution was placed in a 0.2-mm fused silica cell.

III. Experimental Results

A. Morphology. A representative cryo-TEM micrograph of a fresh 0.35 mM C8S3 solution is shown in Figure 2a. The micrograph clearly reveals tubular aggregates, which are slightly bent and typically several hundreds of nanometers long (the bar is 50 nm). Figure 2b shows a section of such a tubular aggregate at larger magnification (the bar is 20 nm), where its double walls are clearly observable. The wall thickness of about 4 nm strongly suggests packing of the dye molecules in a bilayer arrangement. This particular structure can be attributed to the amphiphilic nature of the dye molecule.[7] The strong dispersion forces between the chromophores lead to their stacking within each layer in a plane-to-plane orientation, whereas the attached octyl chains are intercalated between the layers to avoid contact with the surrounding aqueous medium because of the hydrophobic effect. In the electron micrographs, the chromophore layers appear as dark lines, and the interlayer formed by the hydrocarbon chains exhibits less contrast. Upon defocusing, Fresnel diffraction fringes appear at the edges of the tubules. From the calculated optical density profile, tubule diameters of 15.6 ± 0.5 and 10.8 ± 0.5 nm were obtained for the outer and inner chromophore layers, respectively. The tubules are highly monodisperse in diameter.

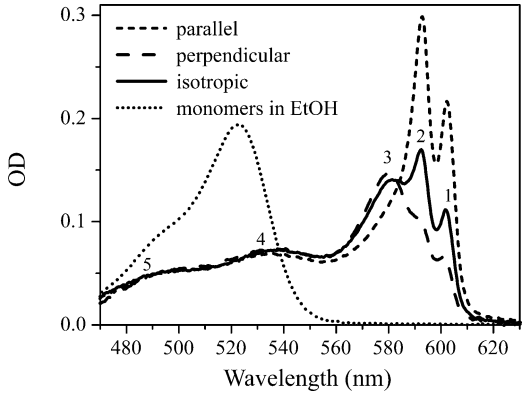

Figure 3. Isotropic (—) and polarized absorption spectra measured with light polarized parallel (- - -) and perpendicular (— — —) to the direction of alignment of C8S3 aggregates in water. The absorption bands are numbered from 1 to 5 starting from lowest energy. The dotted curve gives the absorption spectrum of C8S3 monomers dissolved in ethanol.

B. Linear Absorption and Fluorescence. In Figure 3, isotropic and polarized absorption spectra of the aggregated C8S3/water solution flowed through a 0.1-mm cell are plotted. In addition, the dotted line presents the absorption spectrum of C8S3 monomers dissolved in ethanol. From this figure, it is evident that the isotropic absorption spectrum of C8S3 aggregates is composed of five bands. We number them from 1 to 5 starting from the lowest energy. As is seen, bands 4 and 5 overlap with the vibronic subbands of the monomer absorption spectrum. Moreover, these bands exhibit no polarization behavior (this is seen more clearly in Figure 4 below). This combination of facts strongly suggests that bands 4 and 5 are associated with nonaggregated molecules. Henceforth, we will therefore concentrate on bands 1−3.

Bands 1−3 are red-shifted relative to the monomer absorption spectrum, and they are clearly polarized: bands 1 and 2 with maxima at 602 and 592 nm, respectively, represent transitions with dipole moments oriented parallel to the direction of alignment of the aggregates (presumably the tubule's axis), whereas band 3, centered at 580 nm, corresponds to transitions with dipole moments oriented perpendicular to this axis. We also note that these three bands are narrow compared to those in the monomer spectrum. The above observations clearly suggest that transitions 1−3 should be associated with excitonic J bands of the C8S3 aggregates.

The LD spectrum, shown in Figure 4, clearly reflects the above polarization properties by featuring two positive peaks (1 and 2) and one negative dip (3). The small negative background in the spectral region 500−550 nm either results from an experimental error or indicates that some weakly allowed transitions with oriented transition dipole moments contribute to the absorption in this spectral region. Returning to Figure 3, we also note that the absorption for perpendicularly polarized light is still substantial over the spectral interval where parallel transitions are located and vice versa. For instance, at around 600 nm, the parallel-polarized transition is reduced by only approximately 70% in the perpendicular-polarized spectra. We will return to this issue in section V.

In Figure 5, the fluorescence spectra of C8S3 aggregates (top panel) and monomers (bottom panel) are presented, along with the corresponding isotropic absorption spectra. Because of the large overlap between the fluorescence and absorption spectra of the aggregates, the shape of the fluorescence spectrum is

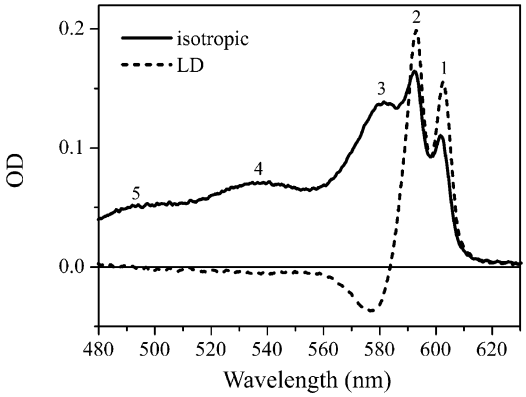

Figure 4. Isotropic absorption (—) and LD (– – –) spectra of C8S3 aggregates.

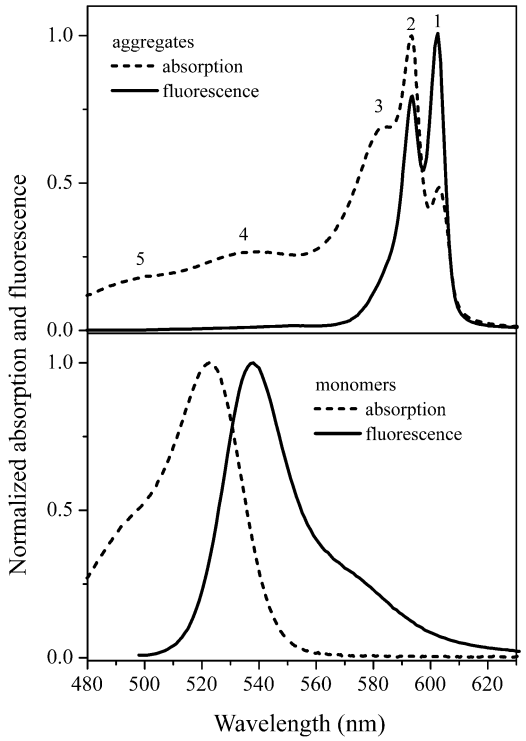

Figure 5. Normalized fluorescence spectra (—) and corresponding absorption spectra (– – –) of C8S3 aggregates (top panel) and monomers (bottom panel).

strongly influenced by reabsorption. Therefore, the fluorescence spectrum was corrected using the equation

$$I(\lambda) = I_r(\lambda)\left[\frac{-\ln(10^{-\mathrm{OD}(\lambda)})}{1-10^{-\mathrm{OD}(\lambda)}}\right] \qquad (1)$$

where $I(\lambda)$ is the true fluorescence, $I_r(\lambda)$ is the recorded fluorescence, and $\mathrm{OD}(\lambda)$ is the optical density of the sample at wavelength λ.

The two fluorescence bands observed in Figure 5 clearly overlap with absorption bands 1 and 2 of the aggregate. In addition, a fluorescence shoulder in the vicinity of 580 nm can be seen. The latter can be related either to absorption band 3 or to a complicated line shape of the fluorescence corresponding to band 2. Finally, a broad and weak fluorescence in the spectral region 540−560 nm might originate from nonaggregated molecules (cf. bottom panel of Figure 5).

The occurrence of two clear fluorescence peaks, overlapping with the two lowest-energy J bands, provides important information about the underlying origin of absorption bands 1 and 2. If these two features originated from excitonic transitions within the same exciton band (i.e., had a common ground state), intraband exciton relaxation would lead to fast relaxation from state 2 to state 1, and no fluorescence associated with high-energy absorption band 2 would be observed. Therefore, the two-peak structure of the fluorescence strongly suggests that we are dealing with two weakly coupled exciton manifolds (also see the Note Added in Proof at the end of the paper). Given the double-wall structure revealed by the cryo-TEM data discussed above, it is natural to assume that bands 1 and 2 should be attributed to two exciton transitions on the inner and outer cylinders that are weakly coupled. It is not clear a priori which transition can be associated with the inner cylinder and which with the outer cylinder (see section V). The absence of a Stokes shift of the fluorescence peaks relative to the absorption peaks 1 and 2 indicates that these transitions are located at the bottom of the two exciton manifolds involved.

Finally, the weak coupling between the two cylinders, although not giving rise to the formation of one collective exciton band, does result in Förster energy transfer between the two cylinders. This is evident from the intensity ratio of the two fluorescence peaks compared to this ratio for the absorption bands. Estimates for the interactions between the two cylinders confirm the picture of weakly coupled cylinders (cf. section IV.B).

IV. Model and Theoretical Considerations

A. Aggregate Structure. Although the cryo-TEM data provide clear insight into the double-wall cylindrical structure of the C8S3 aggregates and the radii of the inner and outer cylinders, the resolution of this technique does not suffice to determine the molecular arrangement within the cylinders. The double-wall structure, however, resembles the planar bilayer structure formed by the closely related C8O4 derivative. Because it is well-accepted that, in a planar geometry, cyanine dye molecules self-assemble into a brick-layer structure,[27−32] it is natural to model the molecular arrangement in both the outer and inner cylinders by wrapping a planar brick-layer lattice onto a cylindrical surface of appropriate radius.

Thus, our starting point is the brick-layer model depicted in Figure 6, with basis vectors $\mathbf{a}_1$ and $\mathbf{a}_2$ (see enlargement on the lower right-hand side). Each unit cell (brick) is occupied by one C8S3 molecule, with its side chains perpendicular to the plane of the lattice. The molecular transition dipole has magnitude μ and is oriented along the molecules' long axis, which lies in the $\mathbf{a}_1$ direction. The length a and width d of the unit cell correspond to the length and thickness, respectively, of the molecule. An important structural parameter is s, which indicates the shift between two adjacent lattice rows in the $\mathbf{a}_1$ direction. This shift determines whether the dominant dipole−dipole interaction (the one between two neighboring molecules) is positive or negative and thereby largely determines whether the aggregate appears as a J or H aggregate.[30] For the purpose of calculating the intermolecular interactions, we model the molecules by extended dipoles, i.e., two point charges separated by a distance l, as is indicated in the upper right-hand side of Figure 6 (see section IV.B for more detail).

We can now wrap the planar brick-layer model onto the surface of a cylinder to obtain a structural model for the tubular aggregate. Many ways exist of doing this, each of which can be uniquely characterized by the wrapping vector **C**, an example of which is indicated in Figure 6. The surface is rolled along the direction of this vector [i.e., the long (z) axis of the cylinder

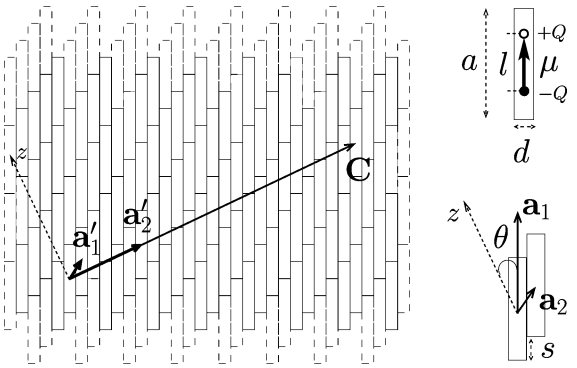

Figure 6. Brick-layer lattice that serves as the basis for the structure of our tubular aggregate model. Each unit cell (dimensions a and d) contains one dye molecule, with its extended dipole μ (length l and charge Q) oriented along the long side of the cell. The lattice can be characterized by the basis vectors $\mathbf{a}_1$ and $\mathbf{a}_2$; two adjacent rows of cells are shifted relative to each other over a distance s. A cylindrical aggregate can be formed from this lattice structure by rolling it onto a cylindrical surface along an arbitrary wrapping vector $\mathbf{C}$ that is commensurate with the lattice periodicity. The cylinder's circumference is thus given by $C = |\mathbf{C}|$, and the direction z perpendicular to $\mathbf{C}$ gives the direction of its long axis. The wrapping angle between this axis and the long side of each unit cell is denoted by θ, which thus gives the angle between the molecular dipoles and the cylinder's axis. The vectors $\mathbf{a}_1'$ and $\mathbf{a}_2'$ are alternative basis vectors, which facilitate viewing the cylinder as a helical stack of rings (see text for details).

is perpendicular to $\mathbf{C}$], and the beginning and ending points should coincide with each other after the rolling process. Hence, the length of $\mathbf{C}$ equals the circumference, $C = 2\pi R$ (where R is the cylinder's radius). Of course, the consistency of the structure requires that, after the brick layer has been rolled onto the cylinder, the bricks at the beginning and ending points exactly overlap, which imposes the condition that $\mathbf{C}$ is a lattice vector

$$\mathbf{C} = t_1\mathbf{a}_1 + t_2\mathbf{a}_2 \tag{2}$$

with t_1 and t_2 integers. Given the values of a, d, and s, this condition implies that R and the angle θ between the z axis and $\mathbf{a}_1$ (this angle fixes the direction of $\mathbf{C}$) cannot take arbitrary values, but can be taken from a discrete set only. Writing out eq 2 along the directions of $\mathbf{C}$ and the z axis, respectively, gives the two relations that define the allowed values for R and θ

$$\begin{cases} t_1 a \sin\theta + t_2 s \sin\theta + t_2 d \cos\theta = 2\pi R \\ t_1 a \cos\theta + t_2 s \cos\theta - t_2 d \sin\theta = 0 \end{cases} \tag{3}$$

We note that, for the aggregates studied in this paper, the discretization of R takes place in very small steps, making it always possible to find a wrapping vector $\mathbf{C}$ that (assuming a, d, and s are fixed) gives a cylinder radius that agrees with the one observed by cryo-TEM within the experimental error.

In principle, the above description completes the general construction of the molecular arrangement in a cylindrical aggregate. In previous work on cylindrical aggregates,[25] two of us argued that an arbitrary cylindrical aggregate can be modeled as a perpendicular stack of equidistant rings, each containing a fixed number of equidistant molecules (N_2) and each subsequent ring rotated with respect to the previous one over a helical angle γ. This stack-of-rings representation has the significant advantage that, in the case of homogeneous aggregates, it allows for a classification of the exciton eigenstates into independent one-dimensional problems, each characterized by a discrete transverse wavenumber k_2. In terms of this wavenumber, simple selection rules can be derived for the optically allowed exciton bands and their polarization directions (see section IV.B for details).

Motivated by these advantages, we map the cylindrical aggregate defined by the wrapping vector $\mathbf{C}$ onto a stack-of-rings representation. We denote by N_2 the number of lattice points intersected by $\mathbf{C}$ (not double counting the first and last point). N_2 is given by the greatest common divisor of t_1 and t_2; in the example of Figure 6, $N_2 = 4$. We now define a new basis vector $\mathbf{a}_2' = \mathbf{C}/N_2$. The other new basis vector $\mathbf{a}_1'$ is then uniquely found from the following conditions: The unit cell must have the same area ($\mathbf{a}_1' \times \mathbf{a}_2' = \mathbf{a}_1 \times \mathbf{a}_2$), $\mathbf{a}_1'$ should reach a lattice point ($\mathbf{a}_1' = p_1\mathbf{a}_1 + p_2\mathbf{a}_2$ with p_1 and p_2 integers), and the projection of $\mathbf{a}_1'$ onto $\mathbf{a}_2'$ should be smaller than $|\mathbf{a}_2'|$. In the new basis ($\mathbf{a}_1'$, $\mathbf{a}_2'$), the vector $\mathbf{a}_2'$ defines the basis vector along rings of N_2 equidistant molecules, while $\mathbf{a}_1'$ defines the direction along helices linking the set of equidistant rings.

Hence, we have mapped the wrapped surface onto a stack of rings. The distance and helical angle between two adjacent rings are given by $h = \mathbf{a}_1' \cdot \hat{\mathbf{z}} = adN_2/(2\pi R)$ and $\gamma = \mathbf{a}_1' \cdot \mathbf{C}/(2\pi R^2)$, respectively. In this representation, each molecule in the cylinder is indicated by the vector $\mathbf{n} = (n_1, n_2)$ giving the decomposition on the basis ($\mathbf{a}_1'$, $\mathbf{a}_2'$). Assuming that the total cylinder has a length of N_1 rings, we have $n_1 = 1, 2, \ldots, N_1$, and $n_2 = 1, 2, \ldots, N_2$. Explicitly, the x, y, and z components of the molecular position vectors and transition dipole moments are given by the three-dimensional vectors

$$\mathbf{r}_\mathbf{n} = [R\cos(n_1\gamma + n_2\phi_2), R\sin(n_1\gamma + n_2\phi_2), n_1 h] \tag{4}$$

and $\boldsymbol{\mu}_\mathbf{n} = \mu\hat{\mathbf{e}}_\mathbf{n}$, with $\hat{\mathbf{e}}_\mathbf{n}$ the unit vector

$$\hat{\mathbf{e}}_\mathbf{n} = [-\sin\theta\sin(n_1\gamma + n_2\phi_2), \sin\theta\cos(n_1\gamma + n_2\phi_2), \cos\theta] \tag{5}$$

with $\phi_2 = 2\pi/N_2$.

B. Exciton Hamiltonian, Eigenstates, and Spectra. We model the optically active electronic states of the tubular aggregates using a Frenkel exciton Hamiltonian. In this Hamiltonian, we neglect the possibility of exciton formation between the inner and the outer cylinders; i.e., for the purpose of calculating the coherent exciton states, we consider the cylinders as electronically decoupled. This approach is motivated from the experimental observations on the fluorescence spectrum described at the end of section III. To provide further support for this picture, we note that the dipole−dipole interaction between a molecule in the inner cylinder and one in the outer cylinder (taking dipoles of 11.4 D, cf. section V) has the maximum value (for a parallel orientation and minimal distance) of 45 cm^{-1}, which is small compared to the observed line width of 150 cm^{-1} of the absorption bands. This suggests that, indeed, exciton transfer between the two cylinders happens via an incoherent Förster mechanism. This transfer will be the topic of a forthcoming study. For the purposes of calculating linear optical spectra, however, this transfer is not of relevance, and we simply model the spectra of the C8S3 tubules as the sum of spectra generated independently by the inner and outer cylinders.

In this section, we thus consider the Frenkel exciton Hamiltonian and the formal results for its states and spectra for a single cylinder with the molecular positions and transition dipoles as described in section IV.A. Setting $\hbar = 1$, this Hamiltonian reads

$$H_0 = \sum_\mathbf{n} \omega_\mathbf{n} b_\mathbf{n}^\dagger b_\mathbf{n} + \sum_{\mathbf{n},\mathbf{m}}{}' J(\mathbf{n}-\mathbf{m}) b_\mathbf{n}^\dagger b_\mathbf{m} \tag{6}$$

where $b_{\mathbf{n}}^{\dagger}$ and $b_{\mathbf{n}}$ denote the Pauli operators for creation and annihilation of an excitation on molecule **n**, respectively.[33,34] Here, the first term describes the molecular excitation energies, where in principle we allow for disorder in the molecular transition frequencies. The second term accounts for the excitation transfer interaction $J(\mathbf{n} - \mathbf{m})$, where the prime on the summation excludes the term with $\mathbf{n} = \mathbf{m}$. We have assumed that this interaction follows the symmetry of the lattice, so that it depends only on the relative positions of the molecules. $J(\mathbf{n} - \mathbf{m})$ is modeled by the interaction between the extended transition dipoles of the molecules **n** and **m**: each dipole is represented as two point charges, $-Q$ and Q, separated by a distance l (Figure 6), and the four interactions between the charges of the molecules involved give the value for $J(\mathbf{n} - \mathbf{m})$. Explicitly, we obtain

$$J(\mathbf{n} - \mathbf{m}) = A\frac{\mu^2}{l^2}\left[\frac{1}{r_{\mathbf{nm}}^{++}} - \frac{1}{r_{\mathbf{nm}}^{+-}} - \frac{1}{r_{\mathbf{nm}}^{-+}} + \frac{1}{r_{\mathbf{nm}}^{--}}\right] \tag{7}$$

where we used $\mu = Ql$ and defined

$$r_{\mathbf{nm}}^{\pm\pm} = |\mathbf{r}_{\mathbf{nm}} \pm l(\hat{\mathbf{e}}_{\mathbf{n}} - \hat{\mathbf{e}}_{\mathbf{m}})/2| \tag{8}$$

$$r_{\mathbf{nm}}^{-+} = |\mathbf{r}_{\mathbf{nm}} - l(\hat{\mathbf{e}}_{\mathbf{n}} + \hat{\mathbf{e}}_{\mathbf{m}})/2| \tag{9}$$

$$r_{\mathbf{nm}}^{+-} = |\mathbf{r}_{\mathbf{nm}} + l(\hat{\mathbf{e}}_{\mathbf{n}} + \hat{\mathbf{e}}_{\mathbf{m}})/2| \tag{10}$$

with $\mathbf{r}_{\mathbf{nm}} = \mathbf{r}_{\mathbf{n}} - \mathbf{r}_{\mathbf{m}}$. The vectors $\mathbf{r}_{\mathbf{n}}$ and $\hat{\mathbf{e}}_{\mathbf{n}}$ are given by eqs 4 and 5, respectively. Finally, $A = 5.04\ \mathrm{cm}^{-1}\ \mathrm{nm}^3/\mathrm{D}^2$.

The exciton eigenstates of the general Hamiltonian eq 6 take the form

$$|\mathbf{k}\rangle = \sum_{\mathbf{n}} \varphi_{\mathbf{k}}(\mathbf{n}) b_{\mathbf{n}}^{\dagger} |g\rangle \tag{11}$$

where $|g\rangle$ denotes the state with all molecules in their ground state, **k** is a general quantum label, and the $\varphi_{\mathbf{k}}(\mathbf{n})$ denote the eigenvectors of the $N \times N$ matrix spanned by the Hamiltonian within the one-exciton subspace ($N = N_1 N_2$). The corresponding eigenvalues $E_{\mathbf{k}}$ give the energy of the state with label **k**.

The general expressions for the absorption and linear dichroism spectra in terms of these eigenvectors and eigenvalues are obtained through standard derivations. We will use the formal expressions for these spectra given in ref 25, which hold independently of the presence of disorder, as long as we realize that **k** represents a general quantum label and not necessarily a wave vector. Without further derivation, we repeat the expressions. For the absorption spectrum taken in an isotropic sample, we have

$$A(\omega) = \sum_{\mathbf{k}} O_{\mathbf{k}} \delta(\omega - E_{\mathbf{k}}) \tag{12}$$

with the oscillator strengths

$$O_{\mathbf{k}} = \langle |\sum_{\mathbf{n}} \varphi_{\mathbf{k}}(\mathbf{n}) \boldsymbol{\mu}_{\mathbf{n}} \cdot \mathbf{e}|^2 \rangle = \sum_{\mathbf{n,m}} \varphi_{\mathbf{k}}(\mathbf{n})\ \varphi_{\mathbf{k}}^{*}(\mathbf{m}) \langle (\boldsymbol{\mu}_{\mathbf{n}} \cdot \mathbf{e})(\boldsymbol{\mu}_{\mathbf{m}} \cdot \mathbf{e}) \rangle \tag{13}$$

Here, $\langle ... \rangle$ represents the isotropic average over the orientations of the cylinder with respect to the polarization vector **e** of the exciting light, and * indicates complex conjugation. The spectrum is a series of peaks at exciton eigenfrequencies, with weights given by the oscillator strengths. Furthermore, assuming that the cylinders are perfectly aligned along their z axes, the linear dichroism spectrum is given by

$$\mathrm{LD}(\omega) = \sum_{\mathbf{k}} L_{\mathbf{k}} \delta(\omega - E_{\mathbf{k}}) \tag{14}$$

with

$$L_{\mathbf{k}} = \sum_{\mathbf{n,m}} \varphi_{\mathbf{k}}(\mathbf{n})\ \varphi_{\mathbf{k}}^{*}(\mathbf{m}) [(\boldsymbol{\mu}_{\mathbf{n}} \cdot \mathbf{z})(\boldsymbol{\mu}_{\mathbf{m}} \cdot \mathbf{z}) - \langle (\boldsymbol{\mu}_{\mathbf{n}} \cdot \mathbf{e}_{\perp})(\boldsymbol{\mu}_{\mathbf{m}} \cdot \mathbf{e}_{\perp}) \rangle] \tag{15}$$

where in the last term $\langle ... \rangle$ denotes the average of the polarization vector $\mathbf{e}_{\perp}$ over all orientations within the xy plane of the cylinders.

In the general case of disordered aggregates, the expressions for the spectra eqs 12 and 14 have to be averaged over the disorder realizations, and their calculation in general requires a fully numerical analysis. This is mostly done through a brute-force simulation of disorder realizations followed by numerical diagonalization of the thus-generated random exciton Hamiltonians. A numerically less expensive alternative is to use the coherent potential approximation (CPA),[35,36] which generally provides very good results for linear absorption spectra (see, e.g., refs 30 and 37−39). As a full simulation of cylindrical aggregates involves diagonalizing large matrices (as each C8S3 cylinder contains thousands of molecules), we have used the CPA to calculate spectra that account for disorder; several results are presented below in section V. More details of these calculations and the excellent agreement of the CPA results with numerically simulated absorption and LD spectra for cylindrical aggregates will be presented in a forthcoming publication.[40]

To end this section, we address the exciton states and spectra in the absence of disorder, i.e., $\omega_{\mathbf{n}} = \omega_0$ for all **n**. The motivation to consider this limit is that it allows for analytical solutions of the exciton states and thus provides simple insights into the type of spectra that can be expected. This limit thus offers important guidance to fit experimental spectra (cf. section V).

In the homogeneous case, the cylindrical symmetry dictates a Bloch form for the dependence of the exciton wave function [$\sim \exp(\mathrm{i}k_2\phi_2 n_2)$, with the transverse quantum number $k_2 = 0$, ± 1, ..., $\pm(N_2/2 - 1)$, $N_2/2$ (see ref 41)] on the position n_2 of the molecule in its ring. This can be used to break down the cylinder's exciton Hamiltonian into N_2 independent effective Hamiltonians for linear systems of length N_1.[25] Only transitions from the cylinder's ground state to states with $k_2 = 0$ or $k_2 = \pm 1$ can appear in the absorption or linear dichroism spectra. Transitions to the $k_2 = 0$ band are always polarized along the long (z) axis of the cylinder and give rise to positive peaks in the LD spectrum. Transitions to the $k_2 = \pm 1$ bands (which are degenerate) are polarized perpendicular to the z axis and lead to negative peaks in the LD spectrum.

If we are dealing with long cylinders, the effective one-dimensional Hamiltonians that result from the decomposition into k_2 bands can be diagonalized by imposing periodic boundary conditions, i.e., by identifying the top and bottom of the cylinder with each other. The eigenstates are then given by

$$\varphi_{\mathbf{k}}(\mathbf{n}) = \frac{1}{\sqrt{N}} \exp[\mathrm{i}(k_1\phi_1 + k_2\phi_2)] \tag{16}$$

with $\phi_1 = 2\pi/N_1$ and $k_1 = 0, \pm 1, ..., \pm(N_1/2 - 1), N_1/2$. The corresponding eigenenergy is given by

$$E_{\mathbf{k}} = \omega_0 + \sum_{\mathbf{n}}{}' J(\mathbf{n}) \cos(k_1\phi_1 + k_2\phi_2) \tag{17}$$

where $J(\mathbf{n})$ is the interaction eq 7 for two molecules separated by a relative position vector $\mathbf{n}$ and the prime on the summation excludes the term with $\mathbf{n} = \mathbf{0}$. The summations over $\mathbf{n}$ must be made in a way consistent with the periodic boundary conditions. In particular, the summation over n_1 extends over $-N_1/2 + 1$, $-N_1/2 + 2$, ..., $N_1/2 - 1$, $N_1/2$.

As has been shown in ref 25, if we impose periodic boundary conditions, only three states contribute to the absorption and LD spectra. These are the states $(k_1, k_2) = (0, 0)$, polarized along the z axis and having energy

$$E_0 = \omega_0 + \sum_{\mathbf{n}}{}' J(\mathbf{n}) \tag{18}$$

and the degenerate states $(k_1, k_2) = (\pm N_1\gamma/2\pi, \pm 1)$, which are polarized perpendicular to the z axis and have energy

$$E_1 = \omega_0 + \sum_{\mathbf{n}}{}' J(\mathbf{n}) \cos(\gamma n_1 + \phi_2 n_2) \tag{19}$$

The fact that only three dipole-allowed transitions occur leads to very simple spectra (cf. ref 25)

$$A(\omega) = \frac{N\mu^2}{3}[\cos^2\theta\, \delta(\omega - E_0) + \sin^2\theta\, \delta(\omega - E_1)] \tag{20}$$

and

$$\mathrm{LD}(\omega) = N\mu^2\left[\cos^2\theta\, \delta(\omega - E_0) - \frac{1}{2}\sin^2\theta\, \delta(\omega - E_1)\right] \tag{21}$$

The only numerical steps involved in calculating these spectra are the summations in eqs 18 and 19.

We end this section by noting that alternative analytical expressions for the exciton wave functions can be obtained that do account for a finite cylinder length.[42] Because the cylinders considered here are very long, we will not pursue that alternative route.

V. Numerical Results and Comparison to Experiment

We now use the model presented in section IV to analyze the experimental spectra reported in section III.B. Here, our main goal is to see whether the wrapped brick-layer model can, in principle, explain the type of spectra that were measured and, if so, what structural model parameters for inner and outer cylinders provide a good reproduction of the experimental spectra.

As argued in section III.B, three exciton bands (1−3) seem to dominate the aggregate spectra, the ones at 602 and 592 nm polarized along the cylinder's long axis and the one at 580 nm polarized perpendicular to it. We use the model results in eqs 20 and 21 as guidance to perform the analysis, where it should be kept in mind that the inner and outer cylinders both contribute an absorption and LD spectrum of this type (one parallel and one perpendicular peak) to the total spectrum. This leads one to tentatively identify the two parallel bands with the parallel transitions of the inner and outer cylinders, whereas the single rather broad perpendicular band observed at 580 nm might result from the fact that the perpendicular transitions of the two cylinders happen to be very close in energy. In recent experiments on the optical properties of aggregates of the dye C8O3, two low-energy absorption bands were also observed with parallel polarization.[10] The higher-energy one of these (corresponding to our transition 2) showed a much stronger sensitivity to changes in the solvent than the lowest-energy band. The same observation was made for the fluorescence bands associated with these two transitions.[10] This strongly suggests that the lowest (highest) parallel transition should be associated with the inner (outer) cylinder. The similarity of the dye C8O3 to the dye C8S3 considered here, as well as the similar morphologies of the two aggregates,[10] suggests that this assignment can be transferred to the C8S3 aggregates. We therefore attribute band 1 (at 602 nm) to an exciton transition in the inner cylinder and band 2 (at 592 nm) to a transition in the outer cylinder.

We now turn to the description of the various system parameters that are either fixed (known from other sources) or free for fitting purposes. To begin, we discuss the structural parameters R, a, d, s, and θ. The cylinder radii were determined from the cryo-TEM experiments reported in section III.A: $R = 7.8$ nm for the outer cylinder and $R = 5.4$ nm for the inner one. We will accept these values as basically fixed, realizing that small deviations (well within the experimental error, vide infra) will be necessary to accommodate the discrete character of R imposed by the underlying brick-layer lattice (see section IV.A). The unit cell dimensions match the size of the chromophore and are fixed at $a = 2.0$ nm[27,28] and $d = 0.4$ nm.[27] The two remaining structural parameters, s and θ, are not known a priori and will be used as free fitting parameters.

The other system parameters are the energetic ones ω_0, Q, and l. For the former, we use $\omega_0 = 18868$ cm^{-1}, which agrees with a single-molecule 0−0 transition at 530 nm (cf. Figure 5). The parameters Q and l together describe the extended dipole that mediates the intermolecular transfer interactions $J(\mathbf{n} - \mathbf{m})$. We take a separation between the charges of $l = 0.7$ nm and a charge of $Q = 0.34e$ (with e the electron charge). These values were obtained from semiempirical calculations[43] and are in good agreement with those obtained for similar dye molecules.[28,44] Combined, these parameters give a single-molecule transition dipole moment of $\mu = 11.4$ D.

We are thus left with two free parameters, s and θ, to fit the experimental results. Although one does not expect very different values for these parameters for the inner and outer cylinders, the larger curvature of the inner cylinder might lead to small discrepancies. For each cylinder, we have to fit the position of the parallel transition as well as the separation between the parallel and perpendicular transitions. Having two independent free parameters per cylinder allows us to do this. Moreover, the ratio of oscillator strengths in the three observed absorption and LD bands should be reproduced, for which no extra free parameters are available.

As we explain in some detail at the end of this section, the position E_0 of the parallel transition is almost independent of θ, due to the fact that the cylinders exhibit a small curvature on the scale of a few lattice unit cells. As this position strongly depends on s through the nearest-neighbor interaction, s can be obtained by fitting it to experiment. On the other hand, we also show at the end of the section that the detuning $E_1 - E_0$ between the parallel and perpendicular transitions of a given cylinder strongly depends on θ, implying that this quantity can be used to determine θ once s has been obtained.

These properties greatly help in establishing relations between structure and spectra and simplify the determination of values for s and θ that give a good match between positions, oscillator strengths, and polarization directions of the exciton transitions in the model with the bands 1−3 found in the experiment of Figure 4. Figure 7 presents the model absorption and LD spectra for such a favorable choice of parameters: $s = 0.242a$ and $\theta = 43.0°$ for the outer cylinder and $s = 0.252a$ and $\theta = 47.4°$ for the inner one. The finite line widths in this figure were obtained by convoluting the theoretical stick spectra eqs 20 and

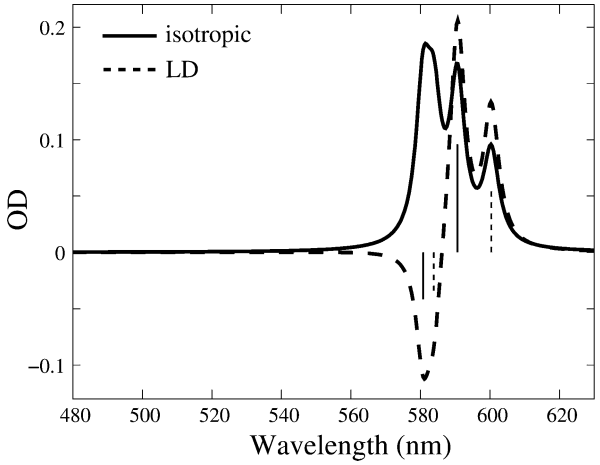

Figure 7. Calculated absorption (—) and LD (− − −) spectra for a homogeneous system of two noninteracting concentric cylindrical aggregates in the infinite-length limit, with model parameters as given in Table 1. The spectra were calculated by convoluting the stick spectra eqs 20 and 21 with Lorentzians of fwhm = 150 cm^{-1}. The sticks shown give the LD strength of the underlying exciton transitions, with solid (dashed) sticks associated with the outer (inner) cylinder. Positive sticks result from states with $k_2 = 0$ and negative ones from those with $k_2 = \pm 1$.

TABLE 1: Summary of Model Parameters that Generate the Spectra in Figure 7,[a] Where Disorder Is Neglected and Stick Spectra Are Convoluted with Lorentzians of fwhm = 150 cm^{-1}

	inner cylinder	outer cylinder
R	5.455 nm	7.833 nm
a	2.0 nm	2.0 nm
d	0.4 nm	0.4 nm
s	0.488 nm	0.508 nm
θ	47.4°	43.0°
ω_0	18868 cm^{-1}	18868 cm^{-1}
l	0.7 nm	0.7 nm
Q	0.34e	0.34e

[a] The same parameters, except that ω_0 is changed to 19194 cm^{-1}, generate Figure 8, where diagonal disorder of standard deviation 670 cm^{-1} is used to generate spectral line widths.

21 with a Lorentzian line shape with full width at half-maximum of 150 cm^{-1} (homogeneous broadening) and transforming to a wavelength scale, $A(\lambda) = A(\omega)\, d\omega/d\lambda$, and analogously for the LD. The stick spectra account for all dipole−dipole interactions within each cylinder.

Comparing Figures 4 and 7, we observe that the general features of the experimental absorption and LD spectra are explained rather well by the simple homogeneous double-wall cylinder model. The main discrepancy is related to band 3, whose width is underestimated in the model result. It is clear from the stick spectra that, indeed, this band results from close-lying perpendicular transitions in the inner and the outer cylinders. The LD dip associated with these transitions, though occurring at the correct frequency, is somewhat overestimated by the homogeneous model. Nevertheless, it is clear that this simple model captures the main features of the spectra, giving support to the structural model and parameters.

For convenience, a summary of the model parameters used is given in Table 1, where we also give the fine-tuned values for the cylinder radii of $R = 7.833$ and 5.455 nm that conform with the discreteness condition eq 3. Within the experimental errors, these values indeed show excellent agreement with the cryo-TEM results of section III.A. The number of molecules N_2 per ring is 5 in the outer cylinder and 2 in the inner one.

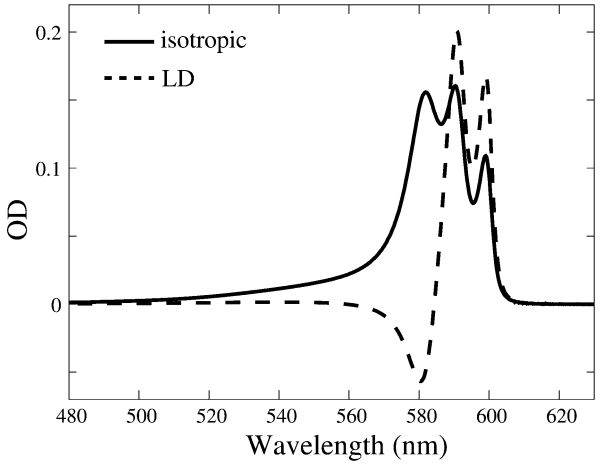

Figure 8. As in Figure 7, except that now the line widths derive from static diagonal disorder of standard deviation $\sigma = 670$ cm^{-1}. The spectra were obtained using the coherent potential approximation (CPA) in the limit of long cylinders.

These numbers are so low because of the low commensurability of the coordinates t_1 and t_2 of the rolling vector **C**; the values for the inter-ring separation h are correspondingly small (0.081 and 0.047 nm, respectively). As a consequence, the N_2 values, though useful for theoretical analysis, do not provide intuitive insight into the typical number of molecules one encounters when going around the cylinder's circumference once. This intuition is easier to obtain from the number of molecules on the cylinder surfaces per nanometer of length of the cylinder, given by $2\pi R/ad = N_2/h$. These numbers are 62 for the outer cylinder and 43 for the inner one.

The purely homogeneous model considered thus far, though giving very reasonable results, oversimplifies reality. In general, the line width of aggregate spectra obtains important contributions from static disorder, which also localizes the exciton wave functions on parts of the cylinder surface. The opposite extreme of the purely homogeneous broadening considered above is a model in which the exciton line width derives solely from static disorder. To consider this situation, we calculated the absorption and LD spectra allowing for diagonal disorder. Here, $\omega_{\mathbf{n}} = \omega_0 + \epsilon_{\mathbf{n}}$, with the $\epsilon_{\mathbf{n}}$ chosen independently from a Gaussian distribution with a standard deviation of 670 cm^{-1}. The model parameters were kept identical to those in Table 1, except that the average molecular transition frequency was shifted to 19194 cm^{-1} (521 nm) to compensate for the disorder-induced shift of the band-edge exciton transitions. We note that the disorder strength is small compared to the exciton bandwidth of about 4000 cm^{-1} for both the inner and outer cylinders, implying that the exciton states are still considerably delocalized. This is confirmed by calculating the inverse participation ratio,[45,46] which indicates that the exciton states contributing to the maxima of the parallel absorption peaks are shared by several tens (30−40) of molecules.

The spectra resulting from the model with diagonal disorder, calculated using the CPA, are shown in Figure 8. We observe the same general features of the spectra as for the homogeneous case, but the disorder creates a better resemblance of the line shape to the measured spectra in Figure 4. We see in particular that band 3 obtains a larger disorder-induced width than bands 1 and 2, which agrees with the experiment; also the LD dip related to band 3 now agrees much better with experiment. Overall, the model with static diagonal disorder generates a remarkable similarity to experiment. A remaining discrepancy is that the experimental spectra in Figure 3 show substantial

absorption for perpendicularly polarized light in the interval where parallel transitions are located and vice versa, whereas the theoretical spectra for both polarizations (not shown) do not reveal this effect. This can be explained either from the fact that the cylinders are not perfectly oriented in the polarization-dependent experiments or from a deformation of the cylinder's circumference from a perfect circle. The lowest-symmetry deformation (of wavelength $2\pi R$) mixes the states in the parallel and perpendicular bands of each cylinder and thus leads to transfer of polarization from one band to the other (cf. refs 47 and 48). Using an analysis similar to that applied in ref 48, we have estimated that small deformations of this type (of the order of several percent) can explain the experimental observations.

At the end of this section, we return in more detail to the role of the free parameters s and θ in the positions of the parallel and perpendicular transitions for homogeneous aggregates. As mentioned above, this provides insight into the relation between structure and spectrum and simplifies the determination of fit parameters.

Let us first consider the position of the parallel transition, which in the model is obtained as E_0 defined in eq 18. Because the cylinders' circumferences are much larger than the molecular dimensions, the curvature of the surface in the local surroundings of a molecule is small, even for the inner cylinder. As the interactions with nearest neighbors in the local environment of a molecule contribute most to the summation in eq 18, we conclude that the position of the parallel band should hardly depend on the fact that the brick-layer lattice is wrapped, i.e., it hardly depends on the angle θ. Rather, it depends on the planar geometry of the underlying brick-layer lattice, which is determined by a and d (both fixed) and s (free). In fact, it is well-known that the position of the absorption band of two-dimensional J and H aggregates depends sensitively on s, as s has a strong influence on (even the sign of) the nearest-neighbor interactions.[30] Thus, if a and d are given, the position of the parallel band can be used to find the value for s. We note that the detuning of 10 nm for the two parallel transitions cannot be explained from a difference in curvature of the inner and outer cylinders and requires that different s values be accepted.

Whereas the position of the parallel transition hardly depends on θ, the situation is different for the perpendicular transition. This is clear from the fact that this transition is associated with the wave vector $\mathbf{k} = (\pm N_2\gamma/2\pi, \pm 1)$, which depends on N_2 and on the helical angle γ, which in turn both depend on θ (cf. section IV.A). Using only the dominant interaction in the summations in eqs 18 and 19, which usually is the one between two neighboring molecules connected by the lattice vector $\mathbf{a}_2$ in the brick-layer lattice, allows us to estimate the detuning between the perpendicular and parallel transitions of the individual cylinders. We thus restrict ourselves to $J \equiv J(n_1, n_2)$ with $n_1\mathbf{a}_1' + n_2\mathbf{a}_2' = \mathbf{a}_2$. Projecting the latter identity onto the $\mathbf{C}$ direction and dividing by R yields

$$n_1\gamma + n_2\phi_2 = \frac{s \sin\theta + d\cos\theta}{R} \tag{22}$$

where the left-hand side is exactly the argument of the cosine in eq 19. From this, we find

$$E_1 - E_0 = 8J \sin^2\left(\frac{s \sin\theta + d\cos\theta}{2R}\right) \tag{23}$$

If n_1 or n_2 equals 0, i.e., if $\mathbf{a}_2$ happens to coincide with one of the new lattice vectors, the prefactor 8 should be replaced by 4. The interesting aspect of eq 23 is that it is a monotonic function of θ over the interval [0, atan(s/d)] with a value of $8J \sin^2(d/2R)$ at $\theta = 0$ and a maximum value of $8J \sin^2(\sqrt{s^2+d^2}/2R)$ at $\theta = \text{atan}(s/d)$. Above, when fitting the experimental spectra using the homogeneous model, we used this property to perform an efficient search for the optimal θ values.

VI. Conclusions

In this paper, using a combination of cryo-TEM, optical spectroscopy, and theoretical techniques, we have built a microscopic model for the tubular self-assembled aggregates of C8S3 dye molecules in water. The wall of the tubules exhibits a double-layer structure, which is a consequence of the amphiphilic nature of the dye molecule. Cryo-TEM reveals diameters of 10.8 ± 0.5 and 15.6 ± 0.5 nm for the constituting inner and outer chromophore layers, respectively. In our theoretical analysis, both layers are modeled as brick-layer lattices wrapped on a cylindrical surface. Each unit cell of the lattice is occupied by one molecule. The collective excitations of the molecules, resulting from intermolecular dipole−dipole interactions, are described within a Frenkel exciton model. This microscopic model for the aggregate's structure and collective excitations explains all experimental observations and allows us to determine the structural parameters s (lattice shift) and θ (wrapping angle) that have thus far not been determined by other means (cf. Table 1).

The model leads to two dominant exciton bands for each cylinder, one polarized parallel to the cylinder's long axis and one perpendicular to it. We have shown that the position of the parallel band can be used to determine s from experiment, while the detuning between the parallel and the perpendicular band is sensitive to θ. Our final model results, which include the effect of diagonal disorder, show a good agreement with experiment, in which three exciton bands can be discerned: two parallel ones, one deriving from each layer, and one broader perpendicular one, which derives from overlapping transitions in the two layers. The delocalization area of the optically dominant exciton wave functions is estimated to be several tens of molecules, which, not suprisingly, is smaller than the low-temperature value of about 100 molecules obtained from pump−probe experiments.[22,24]

As noted in the Introduction, the morphology and spectral properties of the substituted 5,5′,6,6′-tetrachlorobenzimidacarbocyanine aggregates depends on the particular attached side groups as well as the solvent. Within the class of tubular aggregates, however, generic features seem to exist, in particular the occurrence of two lowest-energy parallel J bands and one higher-energy perpendicular band. Exact positions and strengths of these transitions are influenced by the choice of side groups and solvent. This suggests that all of these aggregates have the same basic structure, but with changes in the values of the structural parameters. For instance, the addition of methanol during aggregation of C8S3 in aqueous solution gives rise to different tubular aggregates. In a forthcoming publication, a systematic study of the effect of preparation conditions on the aggregates' morphology and spectroscopy will be presented. There, we will also address the CD spectrum. This spectrum seems ideal to further pinpoint the chiral structure of the aggregates and test our model. Experiments reveal, however, that the CD spectrum is extremely sensitive to sample preparation (even to the sample's concentration). At the same time, the calculated CD spectra sensitively depend on the model parameters. In fact, it turns out that, within the range of

parameters that give good fits for the absorption and LD spectra, the experimental variety of CD spectra can be covered completely.

A most interesting perspective of the tubular tetrachlorobenzimidacarbocyanine aggregates is the possibility to use them as nanometer-scale wires for energy transport. Obtaining more insight into this aspect requires investigating the exciton dynamics. This will be done in a forthcoming publication, in which we will present results of time-resolved fluorescence and pump−probe spectroscopy, as well as calculations of the dynamics using the same structural model as presented above. These studies should also cast light on the contribution of intraband and interband exciton relaxation to the width of absorption peak 3 (the perpendicular transitions). The best calculated spectrum (Figure 8) still overestimates the height of this peak and seems to underestimate its width (cf. Figure 3). The lack of a detailed description of relaxation in our present model might well be the cause of this discrepancy.

Acknowledgment. This work is part of the research program of the Stichting voor Fundamenteel Onderzoek der Materie (FOM), which is financially supported by the Nederlandse Organisatie voor Wetenschappelijk Onderzoek (NWO). H.v.B. thanks C. Böttcher for his help in the cryo-TEM experiments and the Deutsche Forschungsgemeinschaft (SFB448 "Mesoskopisch strukturierte Verbundsysteme") for financial support.

Note Added in Proof. In contrast to what we argued in section III.B, the observation of two fluorescence peaks at the same positions as the two lowest-energy absorption peaks is not conclusive proof that we are dealing with two separate exciton bands. At room temperature, thermal equilibrium between the corresponding transitions could equally well give rise to two fluorescence peaks, even if both transitions occur in the same exciton band. A conclusive proof is provided by the observation[49] that pumping in the 602 nm band does not create bleaching of the 592 nm band. In addition, the estimate of the inter-wall interaction in the beginning of section IV.B lends independent theoretical support to the assumption of two weakly-coupled excitonic manifolds.

References and Notes

(1) Hartgerink, J. D.; Zubarev, E. R.; Stupp, S. I. *Curr. Opin. Solid State Mater. Sci.* **2001**, *5*, 355.
(2) Hirschberg, J. H. K. K.; Brunsveld, L.; Ramzi, A.; Vekemans, J. A. J. M.; Sijbesma, R. P.; Meijer, E. W. *Nature* **2000**, *407*, 167.
(3) van Amerongen, H.; Valkunas, L.; van Grondelle, R. *Photosynthetic Excitons*; World Scientific: Singapore, 2000.
(4) McDermott, G.; Prince, S. M.; Freer, A. A.; Hawthornthwaite-Lawless, A. M.; Papiz, M. Z.; Cogdell, R. J.; Isaacs, N. W. *Nature* **1995**, *374*, 517.
(5) Koepke, J.; Hu, X.; Muenke, C.; Schulten, K.; Michel, H. *Structure* **1996**, *4*, 581.
(6) Pawlik, A.; Ouart, A.; Kirstein, S.; Abraham, H.-W.; Dähne, S. *Eur. J. Org. Chem.* **2003**, 3065.
(7) von Berlepsch, H.; Böttcher, C.; Ouart, A.; Burger, C.; Dähne, S.; Kirstein, S. *J. Phys. Chem. B* **2000**, *104*, 5255.
(8) von Berlepsch, H.; Ouart, A.; Regenbrecht, M.; Akari, S.; Keiderling, U.; Schnablegger, H.; Dähne, S.; Kirstein, S. *Langmuir* **2000**, *16*, 5908.
(9) Spitz, C.; Dähne, S. *Ber. Bunsen-Ges. Phys. Chem.* **1998**, *102*, 738.
(10) von Berlepsch, H.; Kirstein, S.; Hania, R.; Didraga, C.; Pugžlys, A.; Böttcher, C. *J. Phys. Chem. B* **2003**, *107*, 14176.
(11) Staehelin, L. A.; Golecki, J. R.; Drews, G. *Biochim. Biophys. Acta* **1980**, *589*, 30.
(12) Betti, J. A.; Blankenship, R. E.; Natarajan, L. V.; Dickenson, L. C.; Fuller, R. C. *Biochim. Biophys. Acta* **1982**, *680*, 194.
(13) Holzwarth, A. R.; Schaffner, K. *Photosynth. Res.* **1994**, *41*, 225.
(14) Prokhorenko, V. I.; Steensgaard, D. B.; Holzwarth, A. R. *Biophys. J.* **2000**, *79*, 2105.
(15) van Burgel, M.; Wiersma, D. A.; Duppen, K. *J. Chem. Phys.* **1995**, *102*, 20.
(16) Rossum, B.-J.; Steensgaard, D. B.; Mulder, F. M.; Boender, G. J.; Schaffner, K.; Holzwarth, A. R.; de Groot, H. J. M. *Biochemistry* **2001**, *40*, 1587.
(17) von Berlepsch, H.; Kirstein, S.; Böttcher, C. *Langmuir* **2002**, *18*, 7699.
(18) Spitz, C.; Knoester, J.; Ouart, A.; Dähne, S. *Chem. Phys.* **2002**, *275*, 271.
(19) DeRossi, U.; Dähne, S.; Meskers, C. J.; Dekkers, P. J. M. *Angew. Chem.* **1996**, *108*, 827.
(20) Spitz, C.; Dähne, S.; Quart, A.; Abraham, H.-W. *J. Phys. Chem. B* **2000**, *104*, 8664.
(21) Kirstein, S.; von Berlepsch, H.; Böttcher, C.; Burger, C.; Ouart, A.; Reck, G.; Dähne, S. *ChemPhysChem* **2000**, *1*, 146.
(22) Bednarz, M.; Knoester, J. *J. Phys. Chem. B* **2001**, *105*, 12913.
(23) Didraga, C.; Knoester, J. *Chem. Phys.* **2002**, *275*, 307.
(24) Lampoura, S. S.; Spitz, C.; Dähne, S.; Knoester, J.; Duppen, K. *J. Phys. Chem. B* **2002**, *106*, 3103.
(25) Didraga, C.; Klugkist, J. A.; Knoester, J. *J. Phys. Chem.* **2002**, *106*, 11474.
(26) Prokhorenko, V. I.; Steensgaard, D. B.; Holzwarth, A. R. *Biophys. J.* **2003**, *85*, 3173.
(27) Czikkely, V.; Försterling, H. D.; Kuhn, H. *Chem. Phys. Lett.* **1970**, *6*, 11.
(28) Czikkely, V.; Försterling, H. D.; Kuhn, H. *Chem. Phys. Lett.* **1970**, *6*, 207.
(29) Nakahara, H.; Fukuda, K.; Möbius, D.; Kuhn, H. *J. Phys. Chem.* **1986**, *90*, 6144.
(30) Bakalis, L. D.; Rubtsov, I.; Knoester, J. *J. Chem. Phys.***2002**, *117*, 5393.
(31) Gil, A.; Möbius, D.; Sández, I.; Suárez, A. *Langmuir* **2003**, *19*, 6430.
(32) Janssens, G.; Touhari, F.; Gerritsen, J. W.; van Kempen, H.; Callant, P.; Deroover, G.; Vandenbroucke, D. J. *Chem. Phys. Lett.* **2001**, *344*, 1.
(33) Agranovich, V. M. *Zh. Exp. Teor. Fiz.* **1959**, *37*, 430 [Engl. transl. *Sov. Phys. JETP* **1960**, *37*, 307]. Agranovich, V. M. *Fiz. Tverd. Tela* **1961**, *3*, 811 [Engl. transl. *Sov. Phys Solid State* **1961**, *3*, 592].
(34) Davydov, A. S. *Theory of Molecular Excitons*; Plenum Press: New York, 1971.
(35) Soven, P. *Phys. Rev.* **1967**, *156*, 809.
(36) Taylor, D. W. *Phys. Rev.* **1967**, *156*, 1017.
(37) Boukahil, A.; Huber, D. L. *J. Lumin.* **1990**, *45*, 13.
(38) Boukahil, A.; Huber, D. L. *J. Lumin.* **1991**, *48*−*49*, 255.
(39) Balagurov, D. B.; La Rocca, G. C.; Agranovich, V. M. *Phys. Rev. B* **2003**, *68*, 045418.
(40) Didraga, C.; Knoester, J. *J. Chem. Phys.*, manuscript submitted.
(41) The upper boundary holds in case N_2 is even. If it is odd, $k_2 = 0, \pm 1, ..., \pm(N_2 - 1)/2$.
(42) Didraga, C.; Knoester, J. *J. Chem. Phys.* **2004**, *121*, 946.
(43) Kirstein, S. Humboldt-Universität, Berlin, Germany. Private communication, 2003.
(44) Norland, K.; Ames, A.; Taylor, T. *Photogr. Sci. Eng.* **1970**, *14*, 295.
(45) Schreiber, M.; Toyozawa, Y. *J. Phys. Soc. Jpn.* **1982**, *51*, 1528; **1982**, *51*, 1537.
(46) Fidder, H.; Knoester, J.; Wiersma, D. A. *J. Chem. Phys.* **1991**, *95*, 7880.
(47) van Oijen, A. M.; Ketelaars, M.; Köhler, J.; Aartsma, T. J.; Schmidt, J. *Science* **1999**, *285*, 400.
(48) Mostovoy M. V.; Knoester, J. *J. Phys. Chem. B* **2002**, *104*, 12355.
(49) Pugžlys, A.; Hania, P. R.; Didraga, C.; Knoester, J.; Duppen, K. *Solid State Phenom.* **2004**, *97*−*98*, 201.